Tilted Dirac cone effects and chiral symmetry breaking in a planar four-fermion model

Y. M. P. Gomes [*] and Rudnei O. Ramos [†]

Departamento de Física Teórica, Universidade do Estado do Rio de Janeiro, 20550-013 Rio de Janeiro, RJ, Brazil

(Received 22 June 2021; revised 16 November 2021; accepted 30 November 2021; published 6 December 2021)

We analyze the chiral symmetry breaking in a planar four-fermion model with non-null chemical potential, temperature, and including the effect of the tilt of the Dirac cone. The system is modeled with a $(2+1)$-dimensional Gross-Neveu-like interaction model in the context of the generalized Weyl Hamiltonian and its phase structure is studied in the mean-field and large-N approximations. Possible applications of the results obtained, e.g., in connection to graphene, are discussed. We also discuss the effect of an external magnetic field applied to the system, which can give rise to the appearance of the anomalous Hall effect and that is expected to arise in connection with two-dimensional Weyl and Dirac semimetals.

DOI: 10.1103/PhysRevB.104.245111

I. INTRODUCTION

Condensed-matter systems, in particular, those with linearly dispersing fermionic excitations, have been serving as perfect platforms for testing predictions made by quantum field theories. This interplay between high-energy physics and condensed matter has been producing new insights about the quantum phenomena. This includes the parallel between the Ginzburg-Landau model of superconductivity and the spontaneous symmetry breaking in the Higgs sector of the standard model of particle physics to the relation between topological insulators and axion electrodynamics, with applications, e.g., in two-dimensional systems [1–7]. The physics of graphene [8] is of particular relevance in this context, where the electrons can be treated in a quasirelativistic way through the Dirac equation in $(2+1)$ dimensions.

Although the relativistic character of the electrons in graphene is intrinsically connected with the Lorentz symmetry, this is not the case in most materials in condensed matter. There are condensed-matter systems where the dispersion in the vicinity of band touching points, even though they can be generically linear and resemble the Weyl equation, they lack Lorentz invariance. Despite the fact that Lorentz symmetry breaking in high-energy physics may emerge in specific contexts [9–15], they face strong constraints in general [15–17]. Despite this, models exhibiting Lorentz symmetry breaking have been recently applied in the condensed-matter area, e.g., as a path to model three-dimensional Weyl semimetals [18–21], quasiplanar organic materials, and heterostructures made of a combination of topological and normal insulators [22–25].

These systems are described by Weyl-like Hamiltonians and, therefore, these systems have quasiparticles that behave like Weyl fermions [26]. These quasiparticles are by construction massless and are more stable against gap formation in comparison to Dirac ones. After several theoretical predictions, the first experimental measurement related to this kind of material [27] shed light on the properties of the first detected Weyl semimetal (for reviews, see, e.g., Refs. [28,29]).

In the present paper, we study how the gapless property associated with Weyl fermions would hold against possible chiral symmetry breaking. Here, the usual Weyl Hamiltonian used in the description of Weyl semimetals [22,23] is extended by the introduction of a four-fermion interaction. The properties of this system are then studied under the effects of both a finite chemical potential and temperature.

Let us recall that four-fermion interacting models, particularly Gross-Neveu (GN)-type models [30] in $(2+1)$ dimensions, are of particular interest. This is because of their simplicity and ability to capture the relevant physics of planar fermionic systems in general and, thus, these types of models have been extensively considered in the literature. These models can have either a discrete chiral symmetry, $\psi \to \gamma_5\psi$, or a continuous one, $\psi \to \exp(i\alpha\gamma_5)\psi$. These types of models have been employed to study, e.g., low-energy excitations of high-temperature superconductors [31], while analogous models with four-fermion interactions have also been used to study the quantum properties of graphene [32]. Taken as an effective low-energy description of the intrinsic physics of many relevant condensed matter systems of interest, the four-fermion models of the GN type have then served as motivation for many previous studies (see, e.g., Refs. [33–41] for different examples of applications). In particular, these models can play a role in understanding the possibility of dynamical gap generation in planar condensed matter systems, e.g., in graphene [32,42–44].

The aim of this paper is then to study a Weyl-like Hamiltonian when it is augmented by a four-fermion interaction of the GN type. We study the interplay between the characteristic anisotropy and tilting of the Dirac cone, as typically considered in these models, with both temperature and chemical potential (i.e., the effects of doping) in the phase structure of the resulting system. This study is performed in the context of the effective potential in the mean-field and large-N

[*] yurimullergomes@gmail.com
[†] rudnei@uerj.br

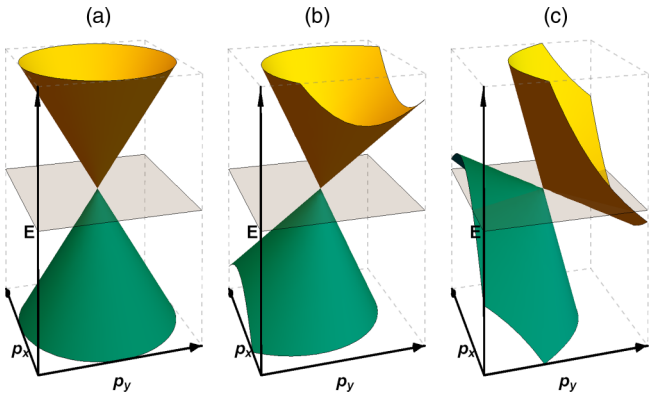

FIG. 1. Illustration of a generic Dirac cone for an isotropic Dirac semimetal (a), type-I Weyl semimetal (b), and type-II Weyl semimetal (c).

approximation. It is expected that this paper will be of interest for learning some of the analogous effects that might be important when considering fermionic quasiparticles and excitonic bound states in planar fermionic systems of relevance.

The remainder of this paper is organized as follows. In Sec. II, we show the relevant properties of two-dimensional Dirac and Weyl semimetal systems. In Sec. III, we extend the model by considering a four-fermion interaction and analyze the effective potential for the averaged value for the chiral operator. The effective potential is derived at the mean-field and large-N level when taking into account the effects of both the anisotropy, tilting of the Dirac cone, chemical potential, and temperature. We dedicate Sec. IV to discuss our results and also some possible applications. In Sec. V, we discuss some expected features for this Weyl-type model when an external magnetic field is applied to the system. Finally, in Sec. VI, we give some additional discussions concerning our results and also our concluding remarks. Throughout this paper, we will be considering the natural units where $\hbar = k_B = c = 1$.

II. TWO-DIMENSIONAL WEYL SEMIMETALS

The generalized Hamiltonian which describes the electrons in the two-dimensional Weyl semimetal (2D WSM) is given by [22,23],

$$H_t(\mathbf{p}) = v_F[(\mathbf{t}\cdot\mathbf{p})\tau^0 + (\xi_x p_x)\tau^x + (\xi_y p_y)\tau^y], \tag{2.1}$$

where v_F is the Fermi velocity, $\tau^0 = \mathbb{I}$ the 2×2 identity matrix, τ^x and τ^y are the Pauli matrices, $\mathbf{t}$ is the vector defining the tilt of the Dirac cone, and $\boldsymbol{\xi} = (\xi_x, \xi_y)$ is the vector that describes the anisotropic character of the crystalline structure. The tilt vector $\mathbf{t}$ is related to the separation between the Dirac cones in the Weyl semimetal. A consequence of the non-null tilt term in Eq. (2.1) is that the Dirac points, denoted by D and D', no longer coincide with the Brillouin corners K and K' (see, e.g., Ref. [23] for details and a review). In particular, type-I Weyl semimetals are characterized by $|\mathbf{t}| < 1$, while type-II ones by $|\mathbf{t}| > 1$ (see Fig. 1 for an illustration). Although $|\mathbf{t}|$ is not restricted, to maintain the physical meaning of the Hamiltonian Eq. (2.1), it is imposed that

$$\sqrt{\left(\frac{t_x}{\xi_x}\right)^2 + \left(\frac{t_y}{\xi_y}\right)^2} = |\tilde{\mathbf{t}}| < 1, \tag{2.2}$$

where $|\tilde{\mathbf{t}}|$ is called the effective tilt parameter. When the condition given by Eq. (2.2) is not respected, the isoenergetic lines are no longer ellipses but instead they are hyperboles [22,23]. The above condition on the effective tilt parameter will also become evident when we give our results for the critical points associated with the chiral symmetry restoration later on. One should also notice that while $|\tilde{\mathbf{t}}|$ is restricted to be smaller than unity, we can still have either the type-I or type-II Weyl cases, $|\mathbf{t}| < 1$ or $|\mathbf{t}| > 1$, respectively, depending on the values for the the anisotropies ξ_x and ξ_y. The value of $|\tilde{\mathbf{t}}|$ depends on the material. For example, in quinoid-type deformed graphene [22], it is of order of 0.6ϵ, with the relative strain parameter $\epsilon < 0.1$ for moderate deformations. The degree of freedom described by the Hamiltonian Eq. (2.1) is that of a (massless) Weyl fermion.

The Hamiltonian spectrum obtained from Eq. (2.1) is given by

$$E(\mathbf{p}) = v_F[\mathbf{t}\cdot\mathbf{p} + \lambda\sqrt{(\xi_x p_x)^2 + (\xi_y p_y)^2}], \tag{2.3}$$

where $\lambda = \pm 1$ define the conduction and valence bands, respectively. Note that the condition Eq. (2.2) ensures the association of $\lambda = +1$ to a positive and $\lambda = -1$ to a negative energy state [22,23]. In the untilted case $t_x = t_y = 0$ and isotropic one, $\xi_x = \xi_y = 1$, we recover the spectrum of isotropic graphene. The Hamiltonian Eq. (2.1) commutes with the chirality operator given by

$$\mathcal{C} = \frac{(\xi_x p_x)\tau_x + (\xi_y p_y)\tau_y}{\sqrt{(\xi_x p_x)^2 + (\xi_y p_y)^2}} \tag{2.4}$$

and the eigenvalues of $\mathcal{C}$ are given by $\alpha = \pm 1$. Due to the twofold degeneracy of the Dirac cones D and D', with representative index $\rho = \pm 1$, the band index can be properly identified as $\lambda = \rho\alpha$. Taking these degeneracies into account, we can write a four-component Weyl spinor ψ and a Dirac-like Lagrangian density can be written as

$$\begin{aligned}\mathcal{L}_0 &= i\bar{\psi}\left[(\partial_t - v_F\mathbf{t}\cdot\boldsymbol{\partial})\gamma^0 - v_F\sum_i(\xi_i\partial_i)\gamma^i\right]\psi \\ &= i\bar{\psi}M^{\mu\nu}\gamma_\mu\partial_\nu\psi,\end{aligned} \tag{2.5}$$

where

$$\gamma^\mu = \tau^\mu \otimes \begin{pmatrix}1 & 0\\ 0 & -1\end{pmatrix}, \tag{2.6}$$

$\tau^\mu = (\tau_3, i\tau_x, i\tau_y)$, and $\bar{\psi} = \psi^\dagger\gamma^0$. The γ-matrices respect the algebra $\{\gamma^\mu, \gamma^\nu\} = 2\eta^{\mu\nu}$ (for details of this representation for fermions in $(2+1)$-dimensions see, e.g., Ref. [45]). We also have that

$$M^{\mu\nu} = \begin{pmatrix}1 & -v_F t_x & -v_F t_y\\ 0 & -v_F\xi_x & 0\\ 0 & 0 & -v_F\xi_y\end{pmatrix}. \tag{2.7}$$

One should note that $M^{\mu\nu}$ contains the parameters that explicitly break the Lorentz symmetry. Note also that we do not

introduce the twofold spin degeneracy here and, in case of interest, we have to double the spinors $\psi \to \psi_s$ for $s = \pm 1$. It is easy to show that the Lagrangian density Eq. (2.5) has a discrete chiral symmetry given by $\psi \to \gamma_5\psi$ and $\bar{\psi} \to -\bar{\psi}\gamma_5$ with [45]

$$i\gamma_5 = \begin{pmatrix} 0 & \mathbb{I} \\ -\mathbb{I} & 0 \end{pmatrix}. \tag{2.8}$$

Though there are some different ways for adding a mass term in the Lagrangian density Eq. (2.5) breaking the chiral symmetry [45], the simplest one is the mass term $\bar{\psi}\psi$. In particular, this mass term can be generated dynamically once the model given by Eq. (2.5) is extended to include a four-fermion interaction of the GN type. This extension is considered next.

III. EXTENDING THE MODEL WITH A FOUR-FERMION INTERACTION

As already mentioned in the Introduction, the use of local four-fermion interactions is well motivated in the literature. These interactions can, for example, describe in an effective way the interaction between electron and phonons in materials [46]. Four-fermion-type interactions can also describe the effects of impurity/disorder [47,48] and, in the case of the GN type of model, it has also been used in the honeycomb lattice searching for the possibility of gap opening [42,49–53]. In addition, these local interactions can be seen as an extension of the BCS theory, effectively describing *s*-wave low-energy interactions, for example. For graphene, for example, in addition to the Coulomb interaction, the effective continuum model for quasiparticles is also expected to contain contact four-fermion interaction terms, which arise from the original lattice tight-binding model [50,54–57]. All these possible interactions, which might be important in opening a gap in 2D systems, are in addition to the long-range Coulomb interaction. There have also been some works modeling the long-range Coulomb interaction in an effective way (see, e.g., Ref. [37]), valid at low energies, through a four-fermion interaction. This could be the case in superconducting materials where the mediating photon for the electron-electron interaction acquires an effective mass. In this case, for momentum less than the effective photon mass, the long-range Coulomb interaction could be effectively approximated by a local contact interaction. In the present paper, we avoid attaching to the interaction any of the above possibilities and use the four-fermion interaction solely as an effective interaction which can work in producing a gap in the system.

For the purpose of analyzing the metal-insulator phase transition in the 2D WSM, the Lagrangian density Eq. (2.5) is extended to include a four-fermion interaction,

$$\mathcal{L} = i\bar{\psi}M^{\mu\nu}\gamma_\mu\partial_\nu\psi + \frac{\lambda v_F}{2N}(\bar{\psi}\psi)^2, \tag{3.1}$$

where ψ is a fermionic field with N flavors (the sum over the flavors implicit) and λ is the coupling constant. Note that the Lagrangian density Eq. (3.1) is still invariant under the discrete chiral symmetry, unless $\langle\bar{\psi}\psi\rangle \neq 0$. Introducing an auxiliary field σ, the Lagrangian density Eq. (3.1) can be equivalently rewritten as

$$\mathcal{L} = \bar{\psi}(iM^{\mu\nu}\gamma_\mu\partial_\nu - \sigma)\psi - \frac{N}{2v_F\lambda}\sigma^2. \tag{3.2}$$

The Lagrangian densities Eqs. (3.1) and (3.2) are completely equivalent. This becomes evident by noticing that the Euler-Lagrange equation of motion for σ and which is obtained from Eq. (3.2) is simply $\sigma = -v_F\lambda/N\bar{\psi}\psi$. When this is substituted back in Eq. (3.2), we recover exactly Eq. (3.1). The GN Lagrangian density expressed in the form of Eq. (3.2) makes evident the chiral operator in terms of the scalar field σ and it is better suitable to study the dynamical fermion mass generation in the model [45].

By integration of the fermionic degree of freedom in the mean-field approximation, where $\sigma_c \equiv \langle\sigma\rangle$ is a constant background field, the effective potential for σ_c, at one-loop order, is given by

$$V_{\text{eff}} = \frac{N}{2v_F\lambda}\sigma_c^2 + \text{tr}\ln(iM^{\mu\nu}\gamma_\mu\partial_\nu - \sigma_c). \tag{3.3}$$

Writing Eq. (3.3) in Euclidean momentum space-time and taking the trace, we find that

$$V_{\text{eff}} = \frac{N}{2v_F\lambda}\sigma_c^2 - 2NT\sum_{n=-\infty}^{+\infty}\int\frac{d^2p}{(2\pi)^2} \times \ln\left[(\omega_n + iv_F\mathbf{t}\cdot\mathbf{p} + i\mu)^2 + v_F^2(\boldsymbol{\xi}\cdot\mathbf{p})^2 + \sigma_c^2\right], \tag{3.4}$$

where $\omega_n = (2n+1)\pi/\beta$ (with $n \in \mathbb{Z}$, $\beta = 1/T$ and T is the temperature of the system) are the Matsubara's frequencies for fermions and μ is the chemical potential. Note that the chemical potential can be interpreted as to account for the extra density of electrons that is supplied to the system by the dopants and, hence, is directly related to the doping concentration. It is also worth pointing out that Eq. (3.4) is an exact result in the large-N approximation [45]. Even though for practical purposes N is finite (e.g., in graphene $N = 2$), we will assume that Eq. (3.4) still provides a sufficiently good approximation as generally assumed in these four-fermion type models [34–37]. We will comment more on the validity of the large-N approximation used here when we discuss our results in the next section.

After summing over the Matsubara's frequencies in Eq. (3.4), we find that the effective potential is given by

$$V_{\text{eff}}(\sigma_c, \mu, T) = \frac{N}{2v_F\lambda}\sigma_c^2 - 2N\int\frac{d^2p}{(2\pi)^2}\left\{E_\sigma + \frac{1}{\beta}\ln\left[1 + e^{-\beta(E_\sigma+\mu)}\right] + \frac{1}{\beta}\ln\left[1 + e^{-\beta(E_\sigma-\mu)}\right]\right\}, \tag{3.5}$$

where

$$E_\sigma = v_F \mathbf{t}\cdot\mathbf{p} + \sqrt{v_F^2\tilde{\mathbf{p}}^2 + \sigma_c^2}, \tag{3.6}$$

with $\tilde{\mathbf{p}}^2 = \tilde{p}_x^2 + \tilde{p}_y^2 \equiv (\boldsymbol{\xi}\cdot\mathbf{p})^2$.

The so-called gap equation is given by

$$\frac{\partial V_{\text{eff}}}{\partial\sigma_c}\Big|_{\sigma_c=\bar{\sigma}_c} = 0, \tag{3.7}$$

which gives

$$1 = 2\lambda v_F \int \frac{d^2p}{(2\pi)^2}\frac{1}{\sqrt{v_F^2\tilde{\mathbf{p}}^2+\bar{\sigma}_c^2}} \times\left[1 - \frac{1}{e^{\beta(E_\sigma+\mu)}+1} - \frac{1}{e^{\beta(E_\sigma-\mu)}+1}\right]\Big|_{\sigma_c=\bar{\sigma}_c}, \tag{3.8}$$

along with the trivial solution $\bar{\sigma}_c = 0$.

Special cases of the above equations will be analyzed next.

A. The $T = \mu = 0$ case

Note that the effective potential Eq. (3.5) is divergent. Considering the limit $\beta\to\infty$ and $\mu\to 0$ in Eq. (3.5) and performing the (divergent) momentum integral with a cutoff Λ, we can define the renormalization condition for the four-fermion interaction λ_R as [35,58]

$$\frac{1}{\lambda_R(m)} = \frac{v_F}{N}\frac{d^2V_{\text{eff}}(\sigma_c)}{d\sigma_c^2}\Big|_{\sigma_c=m} = \frac{1}{\lambda} + \frac{2m}{\pi\xi_x\xi_y v_F} - \frac{\Lambda}{\pi\xi_x\xi_y v_F}, \tag{3.9}$$

where m is a regularization scale. Next, defining the renormalization invariant coupling λ_R as

$$\frac{1}{\lambda_R} = \frac{1}{\lambda_R(m)} - \frac{2m}{\pi\xi_x\xi_y v_F}, \tag{3.10}$$

we arrive at the renormalized effective potential as given by

$$V_{\text{eff,R}}(\sigma_c) = \frac{N}{2v_F\lambda_R}\sigma_c^2 + \frac{N}{3\pi\xi_x\xi_y v_F^2}|\sigma_c|^3. \tag{3.11}$$

When $\lambda_R < 0$, the nontrivial vacuum solution of Eq. (3.11) is given by

$$\bar{\sigma}_c = \sigma_0 \equiv \frac{v_F\pi\xi_x\xi_y}{|\lambda_R|}, \tag{3.12}$$

while for $\lambda_R > 0$ we have that $\bar{\sigma}_c = 0$. Note that

$$V_{\text{eff,R}}(\sigma_c=\sigma_0) = \frac{N(\pi\xi_x\xi_y)^2 v_F}{6\lambda_R^3} \tag{3.13}$$

and, hence, Eq. (3.12) corresponds to the true minimum of the system. We can also see that the value of σ_0 is modified by the dependence on the anisotropy constants, ξ_x, ξ_y, and we recover the usual result [34,35] in the isotropic limit: $\xi_x,\ \xi_y\to 1$. One can further notice here, in the zero temperature and zero chemical potential limits, that the tilt parameter $\mathbf{t}$ does not contribute to the effective potential.

B. The $T = 0$ and $\mu \neq 0$ case

At zero temperature but with a non-null chemical potential, from the effective potential Eq. (3.5) and considering Eq. (2.2), one obtains that

$$V_{\text{eff,R}}(\sigma_c,\mu) = V_{\text{eff,R}}(\sigma_c) - 2N\int\frac{d^2p}{(2\pi)^2}(\mu - E_\sigma)\Theta(\mu - E_\sigma), \tag{3.14}$$

where $\Theta(x)$ is the standard Heaviside function. Even though we cannot explicitly make the integration in the momentum in Eq. (3.14) analytically, we can analyze it when the effective tilt parameter $|\tilde{\mathbf{t}}|$ is small. This is useful to obtain an understanding of the effect of $|\tilde{\mathbf{t}}|$. For a small effective tilt parameter, $|\tilde{\mathbf{t}}| \ll 1$, we can find for Eq. (3.14) the approximated result

$$V_{\text{eff,R}}(\sigma_c,\mu) = V_{\text{eff,R}}(\sigma_c) - \frac{N}{2\pi\xi_x\xi_y v_F^2}\Theta(\mu^2-\sigma_c^2) \times\left[\frac{1}{3}\left(\mu^3 - 3\sigma_c^2\mu + 2|\sigma_c|^3\right) + \frac{1}{2}|\tilde{\mathbf{t}}|^2\mu\left(\mu^2-\sigma_c^2\right)\right] + O(|\tilde{\mathbf{t}}|^4). \tag{3.15}$$

Equation (3.15) shows that the effect of the effective tilt parameter is to enhance the chemical potential. This is confirmed by the results shown in Fig. 2. Figure 2 shows the effective potential as a function of σ_c obtained from the numerical integration of Eq. (3.14) and for some representative values of μ and $|\tilde{\mathbf{t}}|$. By comparing the Figs. 2(a) and 2(b), we can see that the effect of the effective tilt parameter is to lower the point of chiral symmetry restoration. In the presence of the tilt, the chiral symmetry is restored at a lower value for the chemical potential, which is in accordance to what we find from the approximated expression Eq. (3.15). This can be confirmed by determining the critical point μ_c for which the chiral symmetry gets restored.

To derive the critical point μ_c, let us first recall that at a vanishing effective tilt parameter, $|\tilde{\mathbf{t}}| = 0$, the chiral symmetry is restored through a first-order phase transition as has been shown in many previous references (see, e.g., Refs. [59–61]). We can see this explicitly happening in Fig. 2(a). In the absence of the tilt parameter, at $\mu = 0$ the effective potential displays a maximum at $\sigma_c = 0$ and a minimum at $\sigma_c = \sigma_0$. As the chemical potential increases, the minimum remains located at $\sigma_c = \sigma_0$ and with an unchanged value for the effective potential. However, the value of the effective potential at the maximum decreases. This continues to happen until the value $\mu = \sigma_0$ is considered. When $\mu = \sigma_0$, we have that $V_{\text{eff,R}}(\sigma_c = \sigma_0, \mu = \sigma_0) = V_{\text{eff,R}}(\sigma_c = 0, \mu = \sigma_0)$ and the minimum and maximum of the effective potential become degenerate. In fact, at $\mu = \sigma_0$ the whole range $0 \leqslant \sigma_c \leqslant \sigma_0$ becomes degenerate and are minimum points of the effective potential. As the chemical potential increases further, $\mu > \sigma_0$, there will be only one minimum for the effective potential and which is located at $\sigma_c = 0$. The chiral symmetry then becomes restored for $\mu > \sigma_0$. The chiral order parameter, which is represented by the minimum of the effective potential, will then jump discontinuously from $\sigma_c = \sigma_0$ to $\sigma_c = 0$ as we change the chemical potential from $\mu < \sigma_0$ to $\mu > \sigma_0$, with $\mu = \sigma_0$

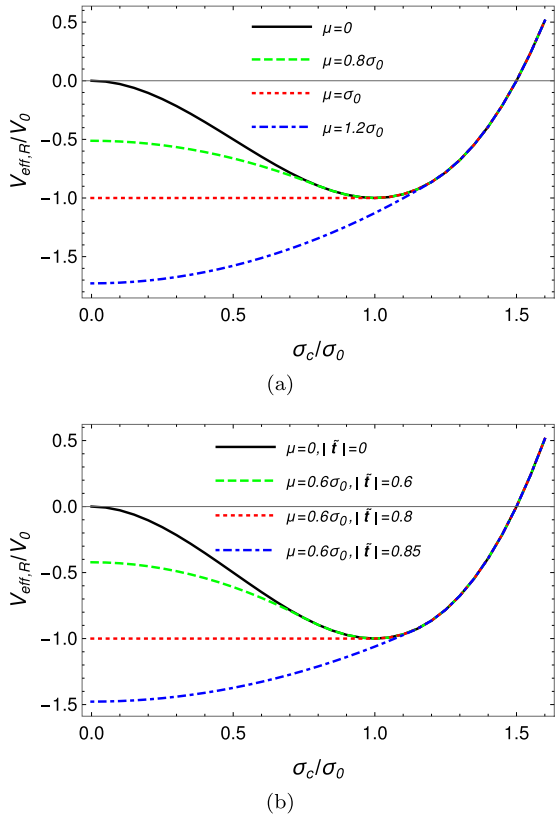

FIG. 2. Normalized plot of the renormalized effective potential at zero temperature, Eq. (3.14), in units of $V_0 \equiv N\sigma_0^3/(6\pi v_F^2 \xi_x \xi_y)$. Panel (a) shows the effective potential when $|\tilde{\mathbf{t}}| = 0$ and for different values for the chemical potential. Panel (b) shows the effect a nonvanishing $|\tilde{\mathbf{t}}|$ in the shape of the effective potential for the chiral order parameter.

representing the critical value for the chemical potential. The discontinuous behavior for the order parameter characterizes the transition as a first-order one. In the presence of the effective tilt parameter, i.e., $|\tilde{\mathbf{t}}| \neq 0$, we can see from Fig. 2(b) that the same trend remains. However, in this case we have that the first-order transition happens at a lower value for the chemical potential. In this sense, we can say that the presence of the nonvanishing tilt parameter facilitates the chiral symmetry restoration.

According to the above discussion, the critical point can then be determined by the condition $V_{\text{eff,R}}(\sigma_c = 0, \mu_c) = V_{\text{eff,R}}(\sigma_c = \sigma_0, \mu_c)$. Using Eq. (3.14), we then find that the critical chemical potential as a function of the effective tilt parameter is given by

$$\mu_c = (1 - |\tilde{\mathbf{t}}|^2)^{1/2}\sigma_0. \tag{3.16}$$

At the critical value μ_c, the potential losses its nontrivial minimum, i.e., $\bar{\sigma}_c(\mu = \mu_c) = 0$. The critical value μ_c as a function of the effective tilt parameter is shown in Fig. 3. For $|\tilde{\mathbf{t}}| = 0$, we recover the known result $\mu_c = \sigma_0$ for the GN model in (2+1) dimensions. The result for the critical μ_c shown in Eq. (3.16) clearly shows that in the presence of a non-null tilt parameter, the gap $\bar{\sigma}_c$ will vanish at a smaller doping and, hence, facilitating the chiral symmetry restoration.

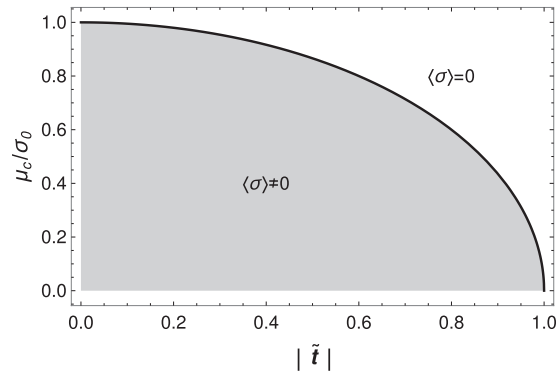

FIG. 3. The critical chemical potential μ_c (in units of σ_0) as a function of $|\tilde{\mathbf{t}}|$.

Note that the tilt parameter also affects the Fermi momentum, which is now given by

$$\tilde{p}_F = \frac{\sqrt{\mu^2 - [1 - |\tilde{\mathbf{t}}|^2 \cos^2(\theta)]\sigma_c^2} - \mu|\tilde{\mathbf{t}}|\cos(\theta)}{v_F[1 - |\tilde{\mathbf{t}}|^2\cos^2(\theta)]}, \tag{3.17}$$

where θ is the angle between $\mathbf{p}_F$ and the tilt vector $\mathbf{t}$. We see that for $-\pi/2 < \theta < \pi/2$, the tilt parameter acts toward increasing the Fermi surface. This is also reflected on the behavior of the charge density n, which is defined as

$$n = -\frac{\partial V_{\text{eff,R}}}{\partial \mu}\bigg|_{\sigma_c = \bar{\sigma}_c}, \tag{3.18}$$

and, using Eq. (3.14), it gives the result

$$n(\sigma_c, \mu) = N\frac{\mu^2 - (1 - |\tilde{\mathbf{t}}|^2)\bar{\sigma}_c^2}{2\pi\xi_x\xi_y v_F^2 (1 - |\tilde{\mathbf{t}}|^2)^{3/2}}\Theta\big[\mu^2 - (1 - |\tilde{\mathbf{t}}|^2)\bar{\sigma}_c^2\big]. \tag{3.19}$$

At the critical value μ_c given by Eq. (3.16), we have that $n(\bar{\sigma}_c = 0, \mu_c) = N\sigma_0^2/(2\pi\xi_x\xi_y v_F^2\sqrt{1 - |\tilde{\mathbf{t}}|^2})$, which is always larger than in the absence of the tilt parameter. This is explicitly seen also in Fig. 4, where Eq. (3.19) is shown as a function of the chemical potential, for a nontilted Dirac cone case and

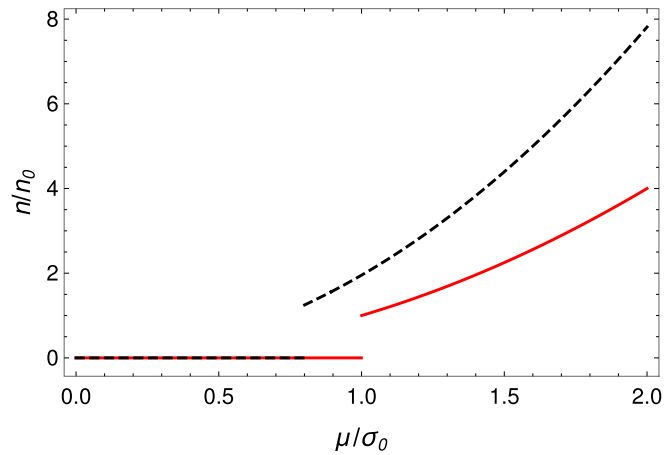

FIG. 4. Density at zero temperature [in units of $n_0 \equiv N\sigma_0^2/(2\pi v_F^2 \xi_x \xi_y)$] as a function of the chemical potential for $|\tilde{\mathbf{t}}| = 0$ (solid line) and for $|\tilde{\mathbf{t}}| = 0.6$ (dashed line).

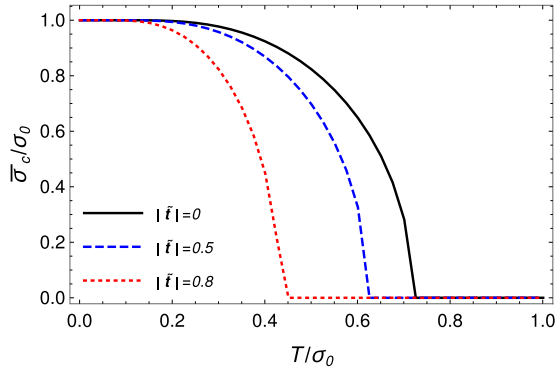

FIG. 5. The chiral order parameter $\bar{\sigma}_c$ as a function of the temperature and for different values for the effective tilt parameter $|\tilde{\mathbf{t}}|$ when $\mu = 0$.

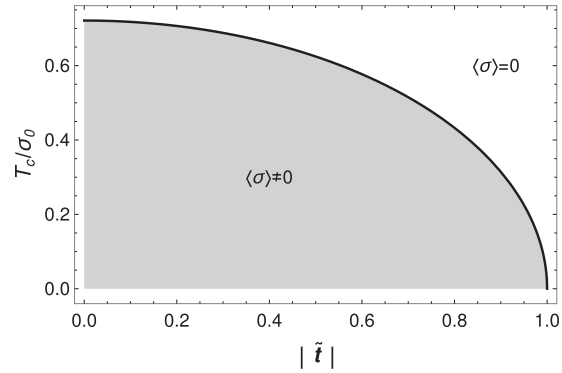

FIG. 6. The critical temperature as a function of $|\tilde{\mathbf{t}}|$ for $\mu = 0$.

also for a tilted one. The discontinuity in the density here is a consequence of the first-order phase transition happening at the critical point μ_c, where the chiral order parameter jumps discontinuously from $\bar{\sigma}_c = \sigma_0$ to $\bar{\sigma}_c = 0$ when going from $\mu < \mu_c$ to $\mu > \mu_c$.

C. $T \neq 0, \mu = 0$

Let us now analyze the case of the chiral symmetry restoration at finite temperature but in the absence of the chemical potential. Taking $\mu = 0$ in Eq. (3.5) and using Eq. (3.11), we then obtain that the renormalized effective potential at finite temperature is given by

$$V_{\text{eff}}(\sigma_c, \mu = 0, T) = \frac{N}{2v_F\lambda_R}\sigma_c^2 + \frac{N}{3\pi\xi_x\xi_y v_F^2}|\sigma_c|^3 - \frac{4N}{\beta}\int\frac{d^2p}{(2\pi)^2}\ln(1 + e^{-\beta E_\sigma}). \quad (3.20)$$

The situation in this case can again be compared to the transition pattern in the GN model in (2+1) dimensions when the tilt effect is absent [59–61]. In that case, the chiral order parameter $\bar{\sigma}_c$ is shown to change continuously from the value σ_0 at $T = 0$ to $\bar{\sigma}_c = 0$ at a critical temperature T_c, which then characterizes the phase transition to be second order. The presence of the tilt does not change this transition pattern, but as in the previous case of $T = 0$ and $\mu \neq 0$, it will lower the critical T_c with respect to the case when $|\tilde{t}| = 0$ as we now show.

The chiral order parameter is obtained from the solution of the saddle point equation

$$\frac{\partial V_{\text{eff,R}}}{\partial\sigma_c}\Big|_{\sigma_c=\bar{\sigma}_c} = 0, \quad (3.21)$$

obtained from the renormalized effective potential. The result is explicitly shown in Fig. 5. In Fig. 5, it is shown the chiral order parameter $\bar{\sigma}_c$ as a function of the temperature and for different values for the effective tilt parameter. We note that $\bar{\sigma}_c$ changes continuously with the temperature. The larger is the effective tilt parameter, the smaller is T_c. The dependence of the critical temperature with the effective tilt parameter is analytical and can be derived directly from Eq. (3.21) when setting $\bar{\sigma}_c = 0$ in that equation. The solution obtained for T_c is then found to be given by

$$T_c = \sqrt{1 - |\tilde{\mathbf{t}}|^2}\,\frac{\sigma_0}{2\ln 2}. \quad (3.22)$$

The behavior of T_c at $\mu = 0$ and as a function of the tilt parameter is shown in Fig. 6.

When $|\tilde{\mathbf{t}}| = 0$, we get the known result for the GN model in (2+1) dimensions [59–61], where $T_c = \sigma_0/(2\ln 2)$. Just like for the previous result for the critical chemical potential, Eq. (3.16), we also see here that the larger the effective tilt parameter, the lower the critical temperature. Once again we see that the effect of the tilt is to facilitate the chiral symmetry restoration, i.e., it can be reached at a lower temperature than in the absence of the tilt.

D. $T \neq 0, \mu \neq 0$

Finally, let us consider the case where both temperature and chemical potential effects are included. The effective potential in this case is given by Eq. (3.5). The critical curve for which $\bar{\sigma}_c(T_c, \mu_c) = 0$ is obtained again from the saddle point equation derived from the renormalized effective potential. In this case, by setting $\bar{\sigma}_c = 0$ in the gap Eq. (3.8), we explicitly find

$$\sigma_0 + \frac{\mu_c - 2T_c\ln\left(e^{\mu_c/T_c} + 1\right)}{(1 - |\tilde{\mathbf{t}}|^2)^{1/2}} = 0, \quad (3.23)$$

which reproduces the result Eq. (3.16) in the zero temperature limit, while at zero chemical potential it leads to the critical temperature as given by Eq. (3.22).

The overall behavior of the critical curve obtained from Eq. (3.23) is shown in Fig. 7. One sees from this figure that the larger the effective tilt parameter, the smaller the region for chiral symmetry breaking. The critical curve in the (T, μ) plane corresponds to a second-order chiral phase transition line. As $T \to 0$, we reach the critical point μ_c as given by Eq. (3.16), which as already discussed above, corresponds to a first-order chiral transition point.

IV. SOME DISCUSSIONS OF THE RESULTS AND APPLICATIONS

As shown from the previous section, in particular, when considering Eqs. (3.16) and (3.22), the results depend directly on the chiral order parameter σ_0. At the same time,

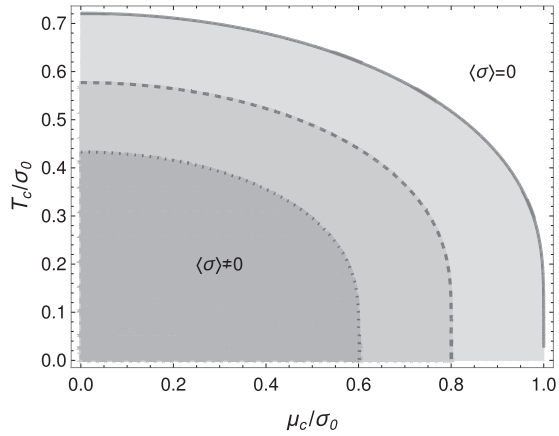

FIG. 7. Critical curve $\bar{\sigma}_c(\mu_c, T_c) = 0$ for $|\tilde{\mathbf{t}}| = 0$ (solid line) and for $|\tilde{\mathbf{t}}| = 0.6$ (dashed line) and $|\tilde{\mathbf{t}}| = 0.8$ (dotted line).

σ_0, which introduces a mass gap in the system, is affected by the anisotropy through the geometric mean Fermi velocity, $v_F^* = \sqrt{\xi_x \xi_y} v_F$. The difference between the effective Fermi velocity v_F^* and the usual one in fully isotropic materials (considering the case of, e.g., graphene, where $v_F \approx c/300$) can alter significantly the critical temperature and critical chemical potential. This is because the dependence of v_F^* on the anisotropies does not have a strong physical bound, such as the one observed by the effective tilt parameter $|\tilde{\mathbf{t}}|$ and given by Eq. (2.2).

It is worth providing some estimates, even though they might be rough ones, based on results obtained from some current planar systems of interest, particularly organic conductors. For illustration purposes, let us consider the case of the recent study [62,63] for the two-dimensional organic conductor $\alpha - (\text{BEDT-TTF})_2 I_3$. From the data provided in Refs. [62,63], the tilt vector $\mathbf{t}$ and anisotropy $\boldsymbol{\xi}$ vector can be estimated to be given (when converted to our notation), respectively, by $\mathbf{t} \simeq (-1.7, 0.3) \times 10^{-4}$ and $\boldsymbol{\xi} \simeq (2.3, 2.4) \times 10^{-4}$, where we have assumed a graphenelike Fermi velocity as a base one (i.e., in the isotropic case). Thus, the effective Fermi velocity is $v_F^* \approx 0.02 v_F$ and the effective tilt parameter can be estimated as $|\tilde{\mathbf{t}}| \approx 0.76$. Therefore, from Eqs. (3.16) and (3.22), the critical chemical potential and critical temperature both get reduced by a factor $\sqrt{1 - |\tilde{\mathbf{t}}|^2 \xi_x \xi_y} \approx 3.6 \times 10^{-8}$ with respect to the untilted and isotropic critical values. This is quite a substantial reduction. This is to be contrasted with the case of quinoid-type graphene under uniaxial strain [22], where $v_F^* \approx v_F$ and the critical temperature and chemical potential of this system can be estimated to decrease by a factor $(1 - 0.02\epsilon^2)$, where ϵ is the relative strain. Given that $\epsilon < 1$ for moderate strain, this leads to a much smaller suppression of μ_c and T_c. Thus, our results indicate that planar organic conductors can remain gapless down to very small temperatures and dopings as a result of the combined effects of anisotropy and the Dirac cone tilt.

There can also be other possible effects of the tilt and anisotropy of the model. Since both the tilt and the anisotropies break the rotational symmetry, there is a possibility that the gap generated is anisotropic in momentum space. The study of such anisotropic solutions and how they would contribute to the problem we have studied would require, however, a study going beyond the proposed methods that we have used in the present paper. In our paper, we have focused on the effects of the tilt and anisotropy in the chiral symmetry breaking and restoration. The use of the effective potential, by definition, only considers field configurations (represented here by the chiral symmetry breaking order parameter σ_c) that are space and time independent. There can be, nevertheless, other contributions to the functional partition function that could contribute and that are solutions of the (nonhomogeneous) field equations. We expect, at least for the present model, those sorts of solutions would cost more energy though (e.g., due to the gradient energy terms) when compared to the constant (homogeneous) field solution contributing to the partition function (and, hence, to the effective potential). It would, of course, be important to explore such solutions, perhaps looking for perturbations to the homogeneous background field solution we have considered. This, of course, would also require a calculation departing from the mean-field approximation we have considered.

Finally, let us comment on the reliability of the large-N expansion used here when applied at the end for systems with as small N. Extending our analysis such as to compute the next order terms in the $1/N$-expansion is generally a difficulty task. But we can take as a basis of the reliability of our results by making a comparison with other works that have already studied the phase diagram of the GN model using alternative approaches to the large-N expansion. For example, in Ref. [64], the phase structure of the GN model in (2+1)-dimensions was studied in the context of the optimized perturbation theory method and which effectively produces results going beyond the large-N expansion. The results obtained in that reference show that both the critical temperature and critical chemical potential are enhanced by a factor $4N/(4N-1)$, which for $N = 2$ means a difference of around 14% percent with respect to the large-N results. Most importantly, those results also have shown that the phase diagram as a whole is qualitatively similar to the one obtained in the large-N limit, except by a small dislocation of the tricritical point to the (T, μ) plane, while in the large-N limit it is located at $(T = 0, \mu = \mu_c)$. Even though we do not expect the large-N approximation to produce precise results for such small values of N, like $N = 2$ as in most of the physical systems of interest, it still produces results of sufficient qualitative agreement and that can provide useful insights on the physics of these systems. This qualitative agreement of the large-N approximation is also seen in other works (e.g., Refs. [65,66]).

V. THE EFFECT OF AN EXTERNAL MAGNETIC FIELD

Let us now discuss some expected effects of coupling the model we have studied to the electromagnetic field. The photon gauge field A_μ couples to the fermions through the standard quantum electrodynamics interaction, $e\bar{\psi}\gamma^\mu\psi A_\mu$. The photon gauge field, when integrated out, produces the Coulomb interaction between the fermions. Note that at the fundamental level, the electromagnetic gauge field can contribute to our results for the effective potential through the fermion polarization term coming from the photon gauge

field and fermion interaction. These fermion polarization contributions are, however, subleading in the large-N approximation. However, the electromagnetic field can (and will be in general) important when acting as an external source. In particular, this can be the case of an external magnetic field applied to the system.

Let us now briefly discuss some possible consequences of adding an external magnetic field to the system. Since the electrons in the 2D Dirac (Weyl) semimetal are charged, we can add a coupling with the electromagnetic sector through the minimal coupling, i.e., $\partial_\mu \to \nabla_\mu = \partial_\mu - ieA_\mu$. The Lagrangian density Eq. (2.5) is then modified as follows:

$$\begin{aligned}\mathcal{L}_0 &= \bar{\psi}(iM^{\mu\nu}\gamma_\mu \nabla_\nu)\psi \\ &= \bar{\psi}(iM^{\mu\nu}\gamma_\mu \partial_\nu)\psi + e\bar{\psi}\gamma_\mu \psi \tilde{A}^\mu, \end{aligned} \tag{5.1}$$

where we have defined an effective electromagnetic potential $\tilde{A}_\mu$ with components

$$\tilde{A}_0 = A_0 - v_F \mathbf{t}\cdot\mathbf{A}, \quad \tilde{A}_i = \xi_{ij}A_j, \quad i = x, y, \tag{5.2}$$

where $\xi_{ij} = \xi_i \delta_{ij}$. Thus, by considering the 2D system in the (x, y) plane and in the presence of an external and constant magnetic field $\mathbf{B}$, we can, without loss of generality, choose a gauge such that the external four-vector potential is given by $A_0 = 0$ and $\mathbf{A}_{3D} = -\frac{1}{2}x\hat{\mathbf{x}} \times \mathbf{B}$. This leads to a magnetic-field component perpendicular to the system's plane, $B_\perp \equiv B_z$ and another component that is parallel to the plane, $B_\parallel \equiv B_y$. Hence, from the tilt vector defined by $\mathbf{t} = (t_x, t_y, 0)$, it is easy to see that Eq. (5.2) can be expressed in the form

$$\tilde{A}_0 = -\tfrac{1}{2}v_F x\hat{\mathbf{x}}\cdot(\mathbf{B}\times\mathbf{t}) = \tfrac{1}{2}v_F x t_x B_\perp. \tag{5.3}$$

Therefore, $B_\perp$ generates a non-null contribution to the time component of the effective vector potential $\tilde{A}_0$ and, thus, the magnetic field will act analogous to an effective external electric field, with magnitude $\tilde{\mathbf{E}}_i = \frac{1}{2}v_F \xi_{ij}(\mathbf{B}\times\mathbf{t})_j$. Besides this, the anisotropy in the spatial direction modifies the magnetic field in the perpendicular direction, $\tilde{B}_\perp = \xi_x\xi_y B_\perp$, while in the parallel direction, $\tilde{B}_\parallel = \xi_y B_\parallel$. Thus, the external magnetic field generates an electrochemical potential given by

$$\tilde{\mu}_s = \mu + \frac{e}{2}v_F x\hat{\mathbf{x}}\cdot(\mathbf{B}\times\mathbf{t}) + \frac{s}{2}g\mu_B|\tilde{\mathbf{B}}|, \tag{5.4}$$

where g is the spectroscopic Landé factor of the electrons ($g \approx 2$ in graphene), $s = \pm 1$, and μ_B is the Bohr magneton.

We can then see that the tilting of the Dirac cone and the anisotropy generates two effects. First, the combination of an external magnetic field and the tilt vector $\mathbf{t}$ generates a non-null chemical affinity $A_i \propto -\nabla_i \mu_s = e(\tilde{\mathbf{E}})_i = \frac{e}{2}v_F B_\perp \xi_{ij}\epsilon^{jk}t_k$ and, therefore, by Onsager reciprocal relations, it will generate a current perpendicular to $\mathbf{t}$. This current will be proportional to $\Phi = \int d^2x B_\perp$. Hence, one can affirm that the 2D Dirac (Weyl) semimetal will have an anomalous Hall effect [67]. Second, the magnetic-field coupling generates an anisotropic Zeeman effect and, therefore, it can be interpreted as an effective giromagnetic term dependent on the direction of the $\mathbf{B}_\parallel$ field. It would be worthwhile to further explore these effects in applications of these type of planar models when subjected to an external magnetic field and which we leave as future work.

VI. CONCLUSIONS

In this paper, we have analyzed the problem of chiral symmetry breaking in a planar four-fermion model when considered in the context of the generalized Weyl Hamiltonian. The GN-like four-fermion interaction provides a way to study the chiral symmetry breaking in the model. The free Hamiltonian that we have employed in this paper was the generalized Weyl one, which includes the anisotropies and the explicit tilting of the Dirac cone. We have then studied how the tilting of the Dirac cone, parameterized by the so-called effective tilt parameter $|\tilde{\mathbf{t}}|$, affects the chiral phase transition as a function of both chemical potential (e.g., doping) and finite temperature. Both the critical temperature and critical chemical potential decrease by a factor $\sqrt{1-|\tilde{\mathbf{t}}|^2}$ with respect to the untilted case. Thus, the tilt parameter suppresses the chiral symmetry breaking, easing its restoration.

Finally, we have shown that the planar fermion system that we have studied will respond to an external magnetic field differently when in the absence or in the presence of the Dirac cone tilt. In the anisotropic and tilted case, there will be an anomalous Hall effect and its magnitude is proportional to the Lorentz-violating parameters $\boldsymbol{\xi}$ and $\mathbf{t}$. This effect changes the effective chemical potential and a current perpendicular to $\mathbf{t}$ appears. The anomalous Hall effect [67] is related to the emergence of this unusual current $\mathbf{j} \propto \mathbf{t}\times\mathbf{B}$. In the model case we have studied, this effect comes from the explicit Lorentz-violating structure of the matrix $M^{\mu\nu}$ in Eq. (5.1). It generates a nonconstant contribution to the chemical potential, which is an explicit character of nonequilibrium systems and which can lead to interesting features in the study of transport phenomena. These and other features found here as a consequence of this paper will be analyzed in more detail in a future work.

ACKNOWLEDGMENTS

Y.M.P.G. is supported by a postdoctoral grant from Fundação Carlos Chagas Filho de Amparo à Pesquisa do Estado do Rio de Janeiro (FAPERJ). R.O.R. is partially supported by research grants from Conselho Nacional de Desenvolvimento Científico e Tecnológico (CNPq), Grant No. 302545/2017-4, and from Fundação Carlos Chagas Filho de Amparo à Pesquisa do Estado do Rio de Janeiro (FAPERJ), Grant No. E-26/201.150/2021.

[1] J. Yu, R. Roiban, S. K. Jian, and C. X. Liu, Finite-scale emergence of 2+1D supersymmetry at first-order quantum phase transition, Phys. Rev. B **100**, 075153 (2019).

[2] P. Gao and H. Liu, Emergent supersymmetry in local equilibrium systems, J. High Energy Phys. 01 (2018) 040.

[3] A. Rahmani, X. Zhu, M. Franz, and I. Affleck, Emergent Supersymmetry from Strongly Interacting Majorana Zero Modes, Phys. Rev. Lett. **115**, 166401 (2015); **116**, 109901(E) (2016).

[4] T. Grover, D. N. Sheng, and A. Vishwanath, Emergent space-time supersymmetry at the boundary of a topological phase, Science **344**, 280 (2014).

[5] L. D. Bernal, P. Gaete, Y. P. M. Gomes, and J. A. Helayël-Neto, Lorentz-symmetry violating physics in a supersymmetric scenario in $(2+1)$-D, Europhys. Lett. **129**, 11005 (2020).

[6] L. Wu, M. Salehi, N. Koirala, J. Moon, S. Oh, and N. P. Armitage, Quantized Faraday and Kerr rotation and axion electrodynamics of the surface states of three-dimensional topological insulators, Science **354**, 1124 (2016).

[7] S. R. Coleman, R. Jackiw, and H. D. Politzer, Spontaneous symmetry breaking in the O(N) model for large N*, Phys. Rev. D **10**, 2491 (1974).

[8] K. S. Novoselov, A. K. Geim, S. V. Morozov, D. Jiang, M. I. Katsnelson, I. V. Grigorieva, S. V. Dubonos, and A. A. Firsov, Two-dimensional gas of massless Dirac fermions in graphene, Nature **438**, 197 (2005).

[9] V. A. Kostelecky and S. Samuel, Spontaneous breaking of Lorentz symmetry in string theory, Phys. Rev. D **39**, 683 (1989).

[10] I. Mocioiu, M. Pospelov, and R. Roiban, Breaking CPT by mixed noncommutativity, Phys. Rev. D **65**, 107702 (2002).

[11] N. E. Mavromatos, Probing Lorentz violating (stringy) quantum space-time foam, AIP Conf. Proc. **1196**, 169 (2009).

[12] N. E. Mavromatos, Lorentz invariance violation from string theory, PoS **(QG-Ph)**, 027 (2007).

[13] D. Colladay and V. A. Kostelecky, CPT violation and the standard model, Phys. Rev. D **55**, 6760 (1997).

[14] D. Colladay and V. A. Kostelecky, Lorentz violating extension of the standard model, Phys. Rev. D **58**, 116002 (1998).

[15] V. A. Kostelecký and N. Russell, Data tables for Lorentz and CPT violation, Rev. Mod. Phys. **83**, 11 (2011).

[16] D. Mattingly, Modern tests of Lorentz invariance, Living Rev. Rel. **8**, 5 (2005).

[17] V. A. Kostelecký and A. J. Vargas, Lorentz and CPT tests with hydrogen, antihydrogen, and related systems, Phys. Rev. D **92**, 056002 (2015).

[18] A. G. Grushin, Consequences of a condensed matter realization of Lorentz violating QED in Weyl semi-metals, Phys. Rev. D **86**, 045001 (2012).

[19] S. Tchoumakov, M. Civelli, and M. O. Goerbig, Magnetic-Field-Induced Relativistic Properties in Type-I and Type-II Weyl Semimetals, Phys. Rev. Lett. **117**, 086402 (2016).

[20] A. A. Soluyanov, D. Gresch, Z. Wang, Q. Wu, M. Troyer, X. Dai, and B. Andrei Bernevig, Type-II Weyl semimetals, Nature **527**, 495 (2015).

[21] X. Wan, A. M. Turner, A. Vishwanath, and S. Y. Savrasov, Topological semimetal and Fermi-arc surface states in the electronic structure of pyrochlore iridates, Phys. Rev. B **83**, 205101 (2011).

[22] M. O. Goerbig, J.-N. Fuchs, G. Montambaux, and F. Piéchon, Tilted anisotropic Dirac cones in quinoid-type graphene and α-$(BEDT-TTF)_2I_3$, Phys. Rev. B **78**, 045415 (2008).

[23] M. O. Goerbig, Electronic properties of graphene in a strong magnetic field, Rev. Mod. Phys. **83**, 1193 (2011).

[24] A. Kobayashi, S. Katayama, Y. Suzumura, and H. Fukuyama, Massless fermions in organic conductor, J. Phys. Soc. Jpn. **76**, 034711 (2007).

[25] S. Katayama, A. Kobayashi, and Y. Suzumura, Pressure-induced zero-gap semiconducting state in organic conductor α-(BEDT-TTF) 2I3 salt, J. Phys. Soc. Jpn. **75**, 054705 (2006).

[26] H. Weyl, Electron and gravitation. 1. (In German), Z. Phys. **56**, 330 (1929).

[27] S. Y. Xu, I. Belopolski, N. Alidoust, M. Neupane, G. Bian, C. Zhang, R. Sankar, G. Chang, Z. Yuan, C. C. Lee *et al.* Discovery of a Weyl Fermion semimetal and topological Fermi arcs, Science **349**, 613 (2015).

[28] N. P. Armitage, E. J. Mele, and A. Vishwanath, Weyl and Dirac semimetals in three dimensional solids, Rev. Mod. Phys. **90**, 015001 (2018).

[29] B. Yan and C. Felser, Topological materials: Weyl semimetals, Annu. Rev. Condens. Matter Phys. **8**, 337 (2017).

[30] D. J. Gross and A. Neveu, Dynamical symmetry breaking in asymptotically free field theories, Phys. Rev. D **10**, 3235 (1974).

[31] W. V. Liu, Parity breaking and phase transition induced by a magnetic field in high T(c) superconductors, Nucl. Phys. B **556**, 563 (1999).

[32] J. E. Drut and D. T. Son, Renormalization group flow of quartic perturbations in graphene: Strong coupling and large-N limits, Phys. Rev. B **77**, 075115 (2008).

[33] H. Caldas, J. L. Kneur, M. B. Pinto, and R. O. Ramos, Critical dopant concentration in polyacetylene and phase diagram from a continuous four-Fermi model, Phys. Rev. B **77**, 205109 (2008).

[34] H. Caldas and R. O. Ramos, Magnetization of planar four-fermion systems, Phys. Rev. B **80**, 115428 (2009).

[35] R. O. Ramos and P. H. A. Manso, Chiral phase transition in a planar four-fermion model in a tilted magnetic field, Phys. Rev. D **87**, 125014 (2013).

[36] K. G. Klimenko and R. N. Zhokhov, Magnetic catalysis effect in the (2+1)-dimensional Gross-Neveu model with Zeeman interaction, Phys. Rev. D **88**, 105015 (2013).

[37] D. Ebert, K. G. Klimenko, P. B. Kolmakov, and V. C. Zhukovsky, Phase transitions in hexagonal, graphene-like lattice sheets and nanotubes under the influence of external conditions, Ann. Phys. **371**, 254 (2016).

[38] D. Ebert, T. G. Khunjua, K. G. Klimenko, and V. C. Zhukovsky, Competition and duality correspondence between chiral and superconducting channels in (2+1)-dimensional four-fermion models with fermion number and chiral chemical potentials, Phys. Rev. D **93**, 105022 (2016).

[39] V. C. Zhukovsky, K. G. Klimenko, and T. G. Khunjua, Superconductivity in chiral-asymmetric matter within the (2 + 1)-dimensional four-fermion model, Moscow Univ. Phys. Bull. **72**, 250 (2017).

[40] N. Zerf, L. N. Mihaila, P. Marquard, I. F. Herbut, and M. M. Scherer, Four-loop critical exponents for the Gross-Neveu-Yukawa models, Phys. Rev. D **96**, 096010 (2017).

[41] L. Fernández, V. S. Alves, M. Gomes, L. O. Nascimento, and F. Peña, Influence of the four-fermion interactions in a (2+1)D massive electron system, Phys. Rev. D **103**, 105016 (2021).

[42] V. Juričić, I. F. Herbut, and G. W. Semenoff, Coulomb interaction at the metal-insulator critical point in graphene, Phys. Rev. B **80**, 081405(R) (2009).

[43] I. F. Herbut, V. Juricic, and O. Vafek, Relativistic Mott criticality in graphene, Phys. Rev. B **80**, 075432 (2009).

[44] H. Rostami and V. Juričić, Probing quantum criticality using nonlinear Hall effect in a metallic Dirac system, Phys. Rev. Research **2**, 013069 (2020).

[45] B. Rosenstein, B. Warr, and S. H. Park, Dynamical symmetry breaking in four Fermi interaction models, Phys. Rept. **205**, 59 (1991).

[46] K. Sasaki and R. Saito, Pseudospin and deformation-induced gauge field in graphene, Prog. Theor. Phys. Suppl. **176**, 253 (2008).

[47] P. L. Zhao, A. M. Wang, and G. Z. Liu, Condition for the emergence of a bulk Fermi arc in disordered Dirac-fermion systems, Phys. Rev. B **98**, 085150 (2018).

[48] J. Wang, Role of four-fermion interaction and impurity in the states of two-dimensional semi-Dirac materials, J. Phys.: Condens. Matter **30**, 125401 (2018).

[49] J. E. Drut and T. A. Lahde, Lattice field theory simulations of graphene, Phys. Rev. B **79**, 165425 (2009).

[50] I. F. Herbut, Interactions and Phase Transitions on Graphene's Honeycomb Lattice, Phys. Rev. Lett. **97**, 146401 (2006).

[51] D. T. Son, Quantum critical point in graphene approached in the limit of infinitely strong Coulomb interaction, Phys. Rev. B **75**, 235423 (2007).

[52] D. E. Sheehy and J. Schmalian, Quantum Critical Scaling in Graphene, Phys. Rev. Lett. **99**, 226803 (2007).

[53] J. E. Drut and T. A. Lahde, Is Graphene in Vacuum an Insulator? Phys. Rev. Lett. **102**, 026802 (2009).

[54] J. Alicea and M. P. A. Fisher, Graphene integer quantum Hall effect in the ferromagnetic and paramagnetic regimes, Phys. Rev. B **74**, 075422 (2006).

[55] I. F. Herbut, Theory of integer quantum Hall effect in graphene, Phys. Rev. B **75**, 165411 (2007).

[56] I. F. Herbut, SO(3) symmetry between Neel and ferromagnetic order parameters for graphene in a magnetic field, Phys. Rev. B **76**, 085432 (2007).

[57] I. L. Aleiner, D. E. Kharzeev, and A. M. Tsvelik, Spontaneous symmetry breakings in graphene subjected to in-plane magnetic field, Phys. Rev. B **76**, 195415 (2007).

[58] A. S. Vshivtsev, K. G. Klimenko, and B. V. Magnitsky, Vacuum structure of the $(\bar{\psi}\psi)^2_3$-model, accounting for the magnetic field and chemical potential, Theor. Math. Phys. **106**, 319 (1996).

[59] K. G. Klimenko, Phase structure of generalized Gross-Neveu models, Z. Phys. C **37**, 457 (1988).

[60] B. Rosenstein, B. J. Warr, and S. H. Park, Thermodynamics of (2+1)-dimensional four Fermi models, Phys. Rev. D **39**, 3088 (1989).

[61] B. Rosenstein, B. J. Warr, and S. H. Park, The Four Fermi Theory is Renormalizable in (2+1)-Dimensions, Phys. Rev. Lett. **62**, 1433 (1989).

[62] M. Hirata, K. Ishikawa, K. Miyagawa, M. Tamura, C. Berthier, D. Basko, A. Kobayashi, G. Matsuno, and K. Kanoda, Observation of an anisotropic Dirac cone reshaping and ferrimagnetic spin polarization in an organic conductor, Nat. Commun. **7**, 12666 (2016).

[63] M. Hirata, A. Kobayashi, C. Berthier, and K. Kanoda, Interacting chiral electrons at the 2D Dirac points: A review, Rep. Prog. Phys. **84**, 036502 (2021).

[64] J. L. Kneur, M. B. Pinto, R. O. Ramos, and E. Staudt, Emergence of tricritical point and liquid-gas phase in the massless $2+1$ dimensional Gross-Neveu model, Phys. Rev. D **76**, 045020 (2007).

[65] J. L. Kneur, M. B. Pinto, R. O. Ramos, and E. Staudt, Updating the phase diagram of the Gross-Neveu model in $2+1$ dimensions, Phys. Lett. B **657**, 136 (2007).

[66] J. L. Kneur, M. B. Pinto, and R. O. Ramos, Phase diagram of the magnetized planar Gross-Neveu model beyond the large-N approximation, Phys. Rev. D **88**, 045005 (2013).

[67] A. A. Burkov, Chiral anomaly and transport in Weyl metals, J. Phys. Condens. Matter **27**, 113201 (2015).